J Seismol
https://doi.org/10.1007/s10950-025-10299-8

RESEARCH

Source parameters of the moderate-sized (ML 4.9) 2018 Arraiolos, Portugal earthquake and its sequence

Piedade Wachilala · José Fernando Borges · Bento Caldeira · Mourad Bezzeghoud

Received: 20 January 2025 / Accepted: 19 May 2025

Abstract The Arraiolos zone is one of the most seismically active intraplate regions in mainland Portugal and is characterized by low- to moderate-magnitude events. However, there is a need to analyse the characteristics of the seismic source parameters in this zone, which is crucial for understanding the origin of the zone's seismicity and gaining insights into the stresses involved in the rupture processes of seismic events. On January 15, 2018, an earthquake of magnitude 4.9 M_L occurred northeast of Arraiolos, near Aldeia da Serra. This event was followed by aftershocks with magnitudes of up to 3.5 (M_L). In the present study, we estimated the source parameters and respective scaling relationships of 82 earthquakes ($0.6 \leq M_L \leq 4.9$) that occurred in the study area following the 2018 Arraiolos earthquake. The source parameters were estimated from the displacement spectra of the P-waves by automatic fitting of the Brune spectral model (ω^{-2}). Consequently, the parameters characterizing the seismic source, such as the scalar seismic moment (M_0), moment magnitude (M_w), corner frequency (f_c), source radius (r_o) and stress drop ($\Delta\sigma$), were determined. The results show that the moment magnitude (M_w) varies between 0.9 and 4.3. The source radii range from 31.5 m to 775.9 m, and the stress drop values ($\Delta\sigma$) range from 0.4 bars to 97.0 bars, with an average of 7.3 bars. Furthermore, most earthquakes occur mainly between 12 and 13 km depth, with a range of stress drop values (including low and high values). The linear relationships between the local and moment magnitudes are consistent. An increasing trend was observed between the source radii and the seismic moments, as expected. It was found that there is no linear correlation between stress drops and seismic moments. This suggests that the dynamic parameters controlling the rupture of larger magnitude earthquakes may be different from those of weaker earthquakes. Studying seismic source parameters in the Arraiolos area is crucial for understanding the seismogenic dynamics, as well as to improve regional hazard assessment.

P. Wachilala (✉)
Department of Exact and Natural Sciences, Higher Institute of Education Science of the Huíla—ISCED-Huíla, Sarmento Rodrigues, nº. 2, Lubango, Angola
e-mail: piedade.wachilala@isced-huila.ed.ao

P. Wachilala · J. F. Borges · B. Caldeira · M. Bezzeghoud
Center for Science and Technology Research in Earth System and Energy (CREATE), University of Évora, Romão Ramalho, nº. 59, 7000-671 Évora, Portugal

J. F. Borges · B. Caldeira · M. Bezzeghoud
School of Science and Technology (SST) of the University of Évora, Romão Ramalho, nº. 59, 7000-671 Évora, Portugal

Published online: 12 June 2025

Highlights

- We estimated the seismic source parameters of the Arraiolos earthquake of January 15, 2018 (M_L 4.9), and its aftershock sequence, which occurred in the Arraiolos region, southern Portugal.
- The distribution of focal depths of earthquakes shows a large concentration mainly between 12 and 13 km, suggesting the presence of the main nucleation zone of these events.
- Large variation of stress drops for different magnitude earthquakes in the same tectonic environment.

Keywords Seismotectonic · Earthquake source parameters · Scaling relationships · Arraiolos Seismic Zone

1 Introduction

On January 15, 2018 at 11:51:40.1 (UTC), a magnitude 4.9 (M_L) earthquake occurred northeast of Arraiolos, with its epicenter near Aldeia da Serra (Lat: 38.783°N, Lon: 7.952°W) at a depth of 12 km (Wachilala et al. 2023). This earthquake occurred along a WNW–ESE-oriented strike-slip fault (Wachilala et al. 2023), and was widely felt in central and southern Portugal, without causing material or human damage. The event reached a maximum intensity (MMI) of VI (strong) in Aldeia da Serra (epicenter area), and an intensity IV/V (moderate) in the city of Évora, located approximately 20 km from the epicenter (Araújo et al. 2020), and also felt with an intensity of III in cities located about 100 km from the epicenter, such as Lisbon. The main shock was followed by a sequence of aftershocks with magnitudes (M_L) $\leq$3.5, which lasted for about a month and a half. This seismic sequence was the best instrumentally recorded in the region and therefore provides a crucial opportunity to understand the seismogenic dynamics of the region.

The study of the spectral parameters of seismic sources is a valuable tool for understanding the geodynamic behaviour of seismic sources and the assessment of seismic hazard. One possible method for estimating earthquake source parameters is the spectral analysis of observed waveforms. To achieve this, various methods are employed to enable accurate and objective interpretations of seismic spectra to provide reliable estimates of source parameters and to establish scaling relationships (e.g., Aki 1967; Haskell 1964; Maruyama 1963; Madariaga 1978; Brune 1970). The simplest and most frequently used source model is described by the low-frequency spectral level Ω_0 and the corner frequency f_c, above which the spectral amplitude is assumed to decay as a second power of the frequency ω^{-2} (Aki 1967; Brune 1970, 1971). The amplitudes of the low frequencies Ω_0 and corner frequency (f_c) acquired from the envelope of the ω^{-2} source seismic spectrum can be used to estimate the seismic moment (M_0) and rupture dimensions; these parameters indicate that the associated stress decreases. The relative movement of tectonic plates causes accumulations of stress along fault systems, which are released during earthquakes (Goebel et al. 2015). The seismic moment M_0 or moment magnitude M_W (Kanamori 1977, 1983; Hanks and Kanamori 1979) is widely considered a reliable measure for quantifying the magnitudes of earthquakes. These parameters reflect the total deformation at the source and are correlated with the release of seismic energy (Kanamori 1983).

Seismic source parameters have been extensively studied worldwide to characterize the sources of local, regional and global earthquakes (e.g., Zobin and Havskov 1995; Ottemöller and Havskov 2003; Allmann and Shearer 2009; Mandal and Dutta 2011; Denolle and Shearer 2016), typically using the Brune spectral model (Brune 1970). The use of P-wave spectra for the determination of seismic source parameters based on the model of Brune (1970) has been adopted in several studies, such as Baumbach and Bormann (2012), Zobin and Havskov (1995), Tusa et al. (2006) for low-magnitude local earthquakes, but also for regional events (Natale et al. 1987) or for teleseismic ones (Hanks and Wyss 1972; Aptekman et al. 1988). The use of P-wave spectra to determine source parameters is advantageous due to their simplicity of identifying the onset of first-arriving phase (Watanabe et al. 1996). Regarding the Arraiolos earthquake of January 15, 2018, several studies have been published in the field of macroseismicity, seismicity and focal mechanisms, and seismic tomography. Araújo et al. (2020) presented a study on the macroseismicity associated with this earthquake and possible implications on the rupture geometry. Wachilala et al. (2023) characterized the seismic activity and focal mechanisms of the Arraiolos Seismic Zone, aiming to propose a seismotectonic model for this region. Recently, Hamak et al. (2025)

conducted the first study on local seismic tomography highlighting the importance of a uniform spatial distribution of earthquakes for obtaining accurate crustal images through seismic inversion. Despite these efforts, there is a need to evaluate the source parameters for the earthquakes in this zone, which is essential for understanding the seismicity pattern and obtaining information about the stresses involved in the rupture processes of seismic events. Furthermore, the source parameters are valuable for future assessments of earthquake hazard in the Arraiolos Seismic Zone.

In this study, we estimate the seismic source parameters of 82 events of the 2018 Arraiolos seismic sequence, which occurred between January 15 and June 30, including the mainshock (M_L 4.9). The study is based on P-waves displacement spectra analysed according the Brune's (1970) circular seismic source model. The dataset covers a magnitude range ($0.6 \leq M_L \leq 4.9$). After corrections for attenuation and site effects, we calculate the various parameters that characterize the source of these events, such as seismic moment, moment magnitude, source size, and stress drop. Additionally, an attempt was made to establish scaling relationships between the source parameters of the modelled events in the region. This research aims to contribute to the understanding of the seismogenesis and the geodynamics of the study area, as well as to improve the assessment of the associated seismic hazard.

2 Geology and seismotectonic setting

The Arraiolos zone, located in the Central Alentejo region in southern mainland Portugal (Fig. 1), is part of the tectonic domain of the Ossa-Morena Zone (OMZ), a tectonic domain that is associated with the Variscan Orogeny that occurred during the upper Paleozoic (480–290 Ma) (Ribeiro et al. 1990). The OMZ is the result of extensional tectonic processes, accompanied by deep crustal metamorphism (Pereira et al. 2015) and magmatism (Ribeiro et al. 1990). The seismotectonic activity of mainland Portugal is generally associated with slow deformation on land (approximately 1 mm/year), driven by the offshore oblique collision between the Eurasian and Nubian tectonic plates, which occurs at a rate of ~5 mm/year (Argus et al. 1989; Borges et al. 2001; DeMets et al. 2010; Bezzeghoud et al. 2012, 2014; Attanayake et al. 2017). Figure 1 illustrates the seismotectonic framework of the Arraiolos region at the regional scale. This area, also referred to as the Arraiolos Seismic Zone, is one of the most significant seismically active intraplate zones in mainland Portugal and is characterized by low- to moderate-magnitude events (most events with $M < 4$, although some events exceed $M > 4$). The seismic activity in this region primarily occurs at depths of 12–15 km (Wachilala et al. 2023).

Studies conducted by Wachilala et al. (2023) indicate that the seismicity in the Arraiolos zone predominantly follows a NW–SE trend. This seismic belt is further divided into three seismic subzones: the Ciborro seismic zone (CSZ), the Aldeia da Serra seismic zone (ASSZ) and the Igrejinha-Azaruja seismic zone (IASZ), with the Aldeia da Serra zone being the main seismic focus (Wachilala et al. 2023). Focal mechanism data from regional events (e.g., Borges 2001; Wachilala et al. 2023) indicate predominantly strike-slip faulting, along with some reverse faulting. These mechanisms, featuring NW–SE-oriented P-axes and NE–SW-oriented T-axes, align with the morphotectonic features observed in this region. The main morphotectonic elements that characterize this area are the Aldeia da Serra escarpment, the São Gregório fault, the Santana do Campo fault and the Ciborro fault (Fig. 2). The mountainous area of Aldeia da Serra consists of a granite massif formed by local tectonic activity. This N–S-oriented morphotectonic feature terminates to the north with a displacement of approximately 100 m caused by the E–W-oriented São Gregório fault, while its southern slope is gentler (Zbyszewski et al. 1979). To the north of the Arraiolos hills lies the Santana do Campo escarpment and the Sabugueiro tectonic gap. The Santana do Campo escarpment, which is of tectonic origin, forms a sharp, linear feature with an elevation difference of 80 m to the north of the Arraiolos hills (Carvalhosa 1999). The Ciborro fault is located within the crystalline massif of Serra de Godeal, at the extreme northwest of Arraiolos. Its scarp is oriented in a NW–SE direction, facing northeast, with elevations ranging from 50 to 60 m (Araújo et al. 2010). On the northern edge of the Serra de Godeal, the Ciborro fault separates the granite formations from the overlying Tertiary substratum.

The main geological formations outcropping in the region (Fig. 2) are predominantly older and cover nearly three-quarters of the area. These formations

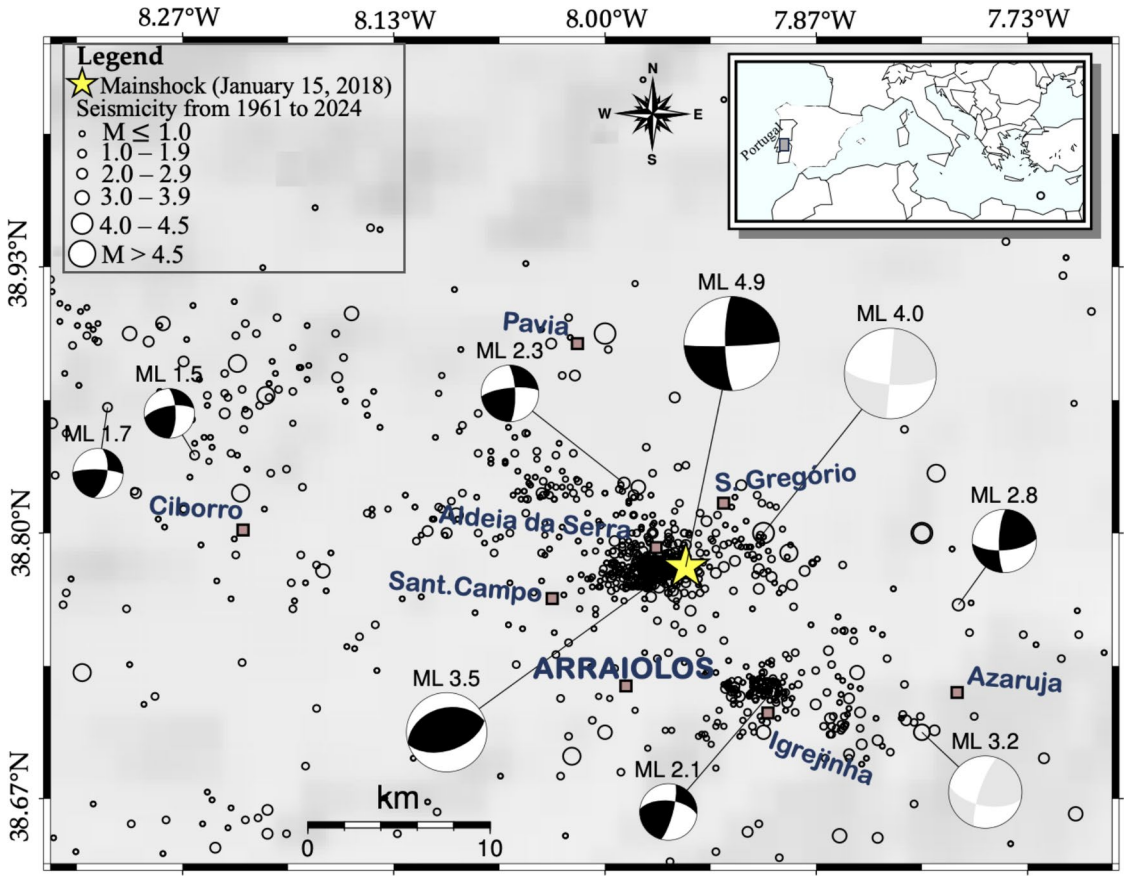

Fig. 1 Distribution of seismicity recorded between 1961 and 2024 in the Arraiolos Seismic Zone, by the Instituto Português do Mar e da Atmosfera (IPMA) and complemented with the events located by Wachilala et al. (2023) from January 15 to June 30, 2018. The yellow star indicates the Arraiolos earthquake of January 15, 2018. The focal mechanisms of some events that indicate the current tectonic regime in the region are also represented. Grey focal mechanisms were determined by Borges et al. (2001). Black focal mechanisms were determined by Wachilala et al. (2023)

consist of crystalline terrains, primarily consisting of a sequence of metamorphic rocks and intrusive (igneous) rocks, with granitoid massifs being the dominant feature. These massifs, roughly concordant with the surrounding terrains, are typically concentrated in late Hercynian macrostructures. The represented rock types include tonalites, quartz diorites, granites, and granodiorites. Additionally, there are subordinate occurrences of gabbro-dioritic and phyllonian rocks, such as microdiorites, microgranites, and pegmatites (Carvalhosa 1999; Pereira et al. 2015). The sedimentary substrates formed during the Tertiary and Quaternary periods are characterized by clayey sediments, conglomerates and limestones. These substrates occupy smaller areas within the region and are mainly concentrated in the northeastern part, extending to the extreme northwest (Zbyszewski et al. 1979; 1980).

3 Data and methods

3.1 Data

In this study, we used a dataset of digital seismic signals that were recorded by 12 broadband stations (Fig. 3) of the Arraiolos network 7N (Fontiela and Bezzeghoud 2018) belonging to the Institute of Earth Sciences (ICT) of the University of Évora. These stations were equipped with Guralp CMG-6 TD/30 s sensors (with a flat response between 0.033 Hz and 50 Hz) and 24-bit digital recording capabilities. The seismic signals

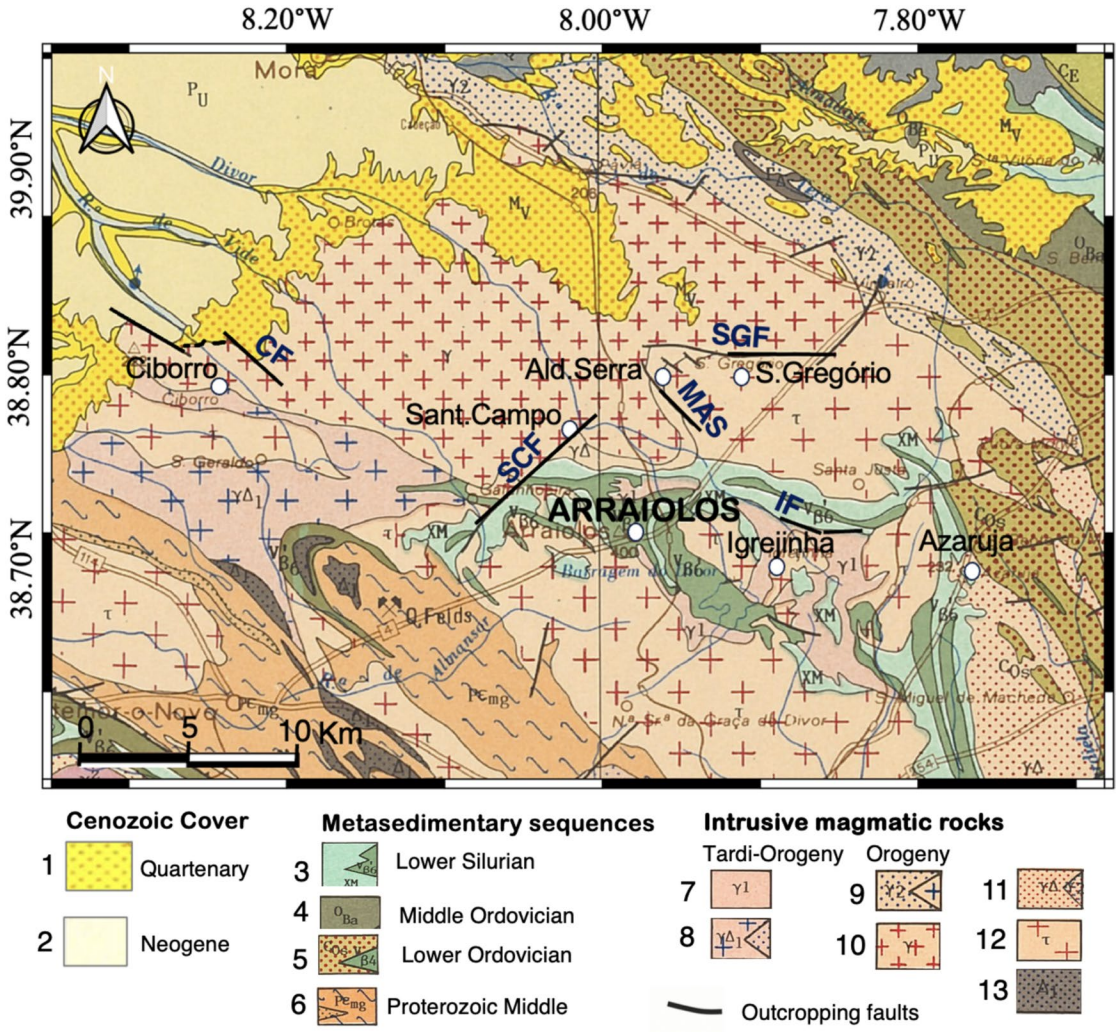

Fig. 2 Geological setting of the study region. *β* Adapted from the Geological Chart of Portugal at a scale of 1/500.000 (Serviços Geológicos de Portugal 1992). 1- Sedimentary 2- Sedimentary; 3- Volcano-sedimentary complex. Phyllites, black schists, quartzites, psammites *XM*; basic volcanites $V\beta_6$; 4- Shists and psammites; 5- Shists, greywackes, and basic volcanites; 6- Migmatized series; amphibolites; 7- Granites; 8- Granodiorites and tonalites; 9- porphyritic two-mica granite; 10- Porphyroid biotite-granites; 11- Granodiorites and granites; 12- Tonalites; 13- Diorites and gabbros. The main outcropping faults observed in this region are represented: *CF* – Ciborro Fault; *SCF* – Santana do Campo Fault; *MAS* – Mountain massif of Aldeia da Serra; *SGF* – São Gregório Fault; *IF* – Igrejinha Fault

were continuously sampled at a frequency of 200 Hz (Wachilala et al. 2023). These stations operated for approximately six months (January 15 − June 30, 2018), following the Arraiolos earthquake of January 15, 2018. Additionally, permanent seismic stations from the national seismic network of IPMA (Instituto Português do Mar e da Atmosfera) and the ICT were utilized. These stations are equipped with broadband seismometers, including Streckheisen STS-2 (120 s/24 bits), Guralp CMG-40 T (30 s/24 bit), and Nanometrics Trillium (120 s/24 bit) models, operating at a sampling rate of 100 Hz. These stations cover a radius of approximately 60 km around the main seismogenic zone of Arraiolos, specifically near Aldeia da Serra.

The data comprises 82 local seismic events recorded between January 15 and June 30, 2018, with magnitudes ranging from $0.6 \leq M_L \leq 4.9$, all exhibiting high all with good signal-to-noise ratios. The epicentres

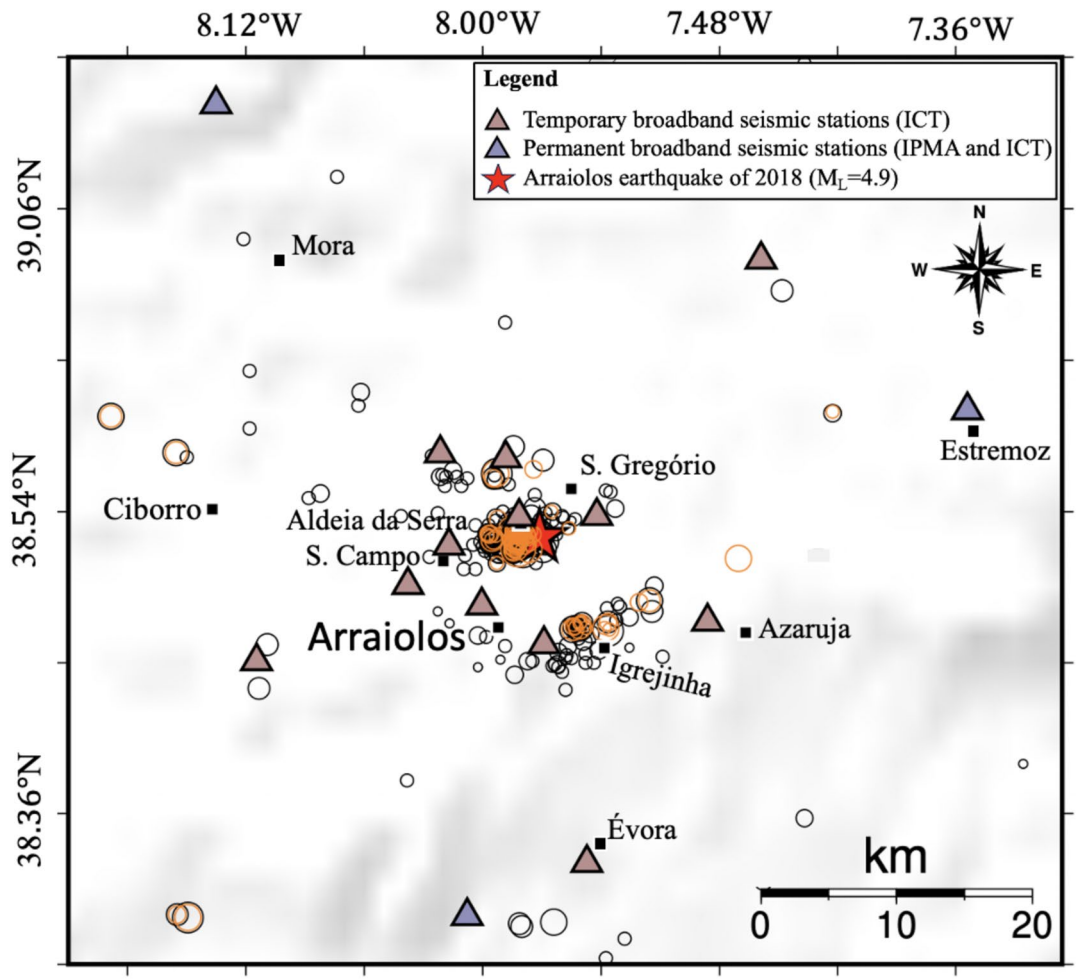

Fig. 3 Epicentral distribution of seismic events that occurred in 2018, located by Wachilala et al. (2023). The orange circles indicate the events analyzed in this study. The red star indicates the 2018 mainshock. The triangles indicate the broadband seismic stations used in this study. Brown triangles: temporary stations of the Institute of Earth Sciences (ICT), University of Évora and blue triangles: permanent stations of IPMA and ICT, respectively

of these events are located in the Arraiolos Seismic Zone and surrounding areas. Figure 3 shows the epicentral distribution of the 82 earthquakes (orange circles) included in our dataset for source spectral analysis, whereas Table 1 (in the appendix) provides the hypocentral parameters of the corresponding seismic events. Detailed information on the hypocentral locations of the entire seismic sequence is available in Wachilala et al. (2023). The uncertainties involved in the estimates of the epicenters and depth are minor that 3 km, and 0.3 s in the origin time (RMS). The focal depth falls in the range of 11.4 to 21.2 km, with depths mainly from 12 to 13 km.

3.2 Methodology

The analysis of seismic source parameters on the basis of the displacement spectra of P-waves was carried out as follows: First, the selected seismic P-wave signals were corrected by removing the mean values. Time windows were selected from the recordings of the vertical components of the P-waves. The time windows employed are in the range of 0.9 s to 4.2 s, starting 0.1 s before the arrival time. The choice of window length depends on the epicentral distance in order to avoid the influence of S-waves. A 10% cosine taper was applied to both ends of the window.

The displacement spectra were then calculated using the fast Fourier transform (FFT). The spectra were subsequently corrected for the instrumental response, and attenuation corrections were applied, based on the observations of Pujades et al. (1990), who investigated the seismic wave attenuation throughout the Iberian Peninsula. In the region covering the study area, $Q_0 = 300$. We assume the relationship $Q_0(f) = 300\ f^{0.70}$.

3.3 Determination of source parameters

The seismic source parameters were estimated using Brune's circular source model (1970). The displacement amplitude spectra were obtained from the P-wave spectra and fitted to the Brune source model and can be expressed (Brune 1970, 1971) as:

$$S(f) = \frac{M_0 F}{\left(1 + (\frac{f}{f_c})^2\right)\left(4\pi\rho v^3\right)} G(\Delta, h) D(f) \quad (1)$$

where M_0 is the seismic moment (Nm), F is a factor of 2.0 ×0.6 to account for the effect of the free surface and the radiation pattern, G(Δ,h) is geometric spreading, Δ is the epicentral distance (km), h is the hypocentral depth (km), D(f) is the attenuation function due to anelastic attenuation, f is the frequency (Hz), ρ is the density (g/cm^3), v is the velocity at the source (km/s) of the P wave or S wave (depending on the spectrum of the wave to be used), and f_c is the corner frequency (Hz).

The attenuation function D(f) is expressed as:

$$D(f) = \mathrm{A}(f) e^{-\pi f k} e^{\frac{-\pi f t}{Q(f)}} \quad (2)$$

where A(f) is the low-frequency spectral level, κ is the high-frequency attenuation factor for the near surface, t is the travel time (time from the origin to the start of the spectral window), and Q(f) is the quality factor that accounts for seismic wave attenuation. The near-surface attenuation, represented by the κ factor, was estimated using the method of Havskov and Ottemöller (2010). The method essentially consists of fitting a straight line to the flat part of the displacement spectrum where $f < f_c$ (frequencies below the likely corner frequency). Thus, the κ factor was determined from the slope of the logarithmic displacement spectrum. The κ values applied in this study range from 0.012 to 0.034 s.

In this study, the spectral parameters were automatically fitted following the methodology proposed by Ottemöller and Havskov (2003) using the SEISAN analysis software (Ottemöller et al. 2016). Using the Brune source model (Brune 1970), the observed spectra were matched to a theoretical curve defined by two parameters: the low-frequency amplitude spectral level Ω_0 and the corner frequency f_c. From these parameters, the remaining seismic source characteristics, such as the seismic moment M_0, moment magnitude M_w, seismic source radius r_0 and stress drop Δσ, were derived using the equations of Brune (1970, 1971) and Kanamori (1977; Hanks and Kanamori 1979) as follows:

$$M_0 = \frac{\Omega_0 4\pi\rho v^3}{0.2 \times 6.0 \times G(\Delta, h)} \quad (3)$$

where Ω_0 is the amplitude level of the spectrum at low frequencies.

$$r_0 = K_p v_p / f_c \quad (4)$$

where v is the velocity P (in km/s) and the constant K_p is 0.50 for the P-wave (Brune 1970).

$$\Delta\sigma = \frac{7}{16} \times \frac{M_0}{r_0^3} \quad (5)$$

$$M_w = \frac{2}{3} \times log10(M_0) - 6.06 \quad (6)$$

The seismic moment (M_0) was calculated in Nm, the source radius (r_0) in km and the stress drop (Δσ) in bars.

4 Results and discussion

4.1 Results

Figure 4 show examples of the displacement spectra that were estimated from the best-fit P waves, in accordance with the ω^2 theoretical model (Brune 1970). Figure 5 shows some examples of displacement spectra obtained from one station for four earthquakes of different magnitudes, with the respective moment magnitudes and corner frequencies determined, illustrating the variation of f_c for Mw.

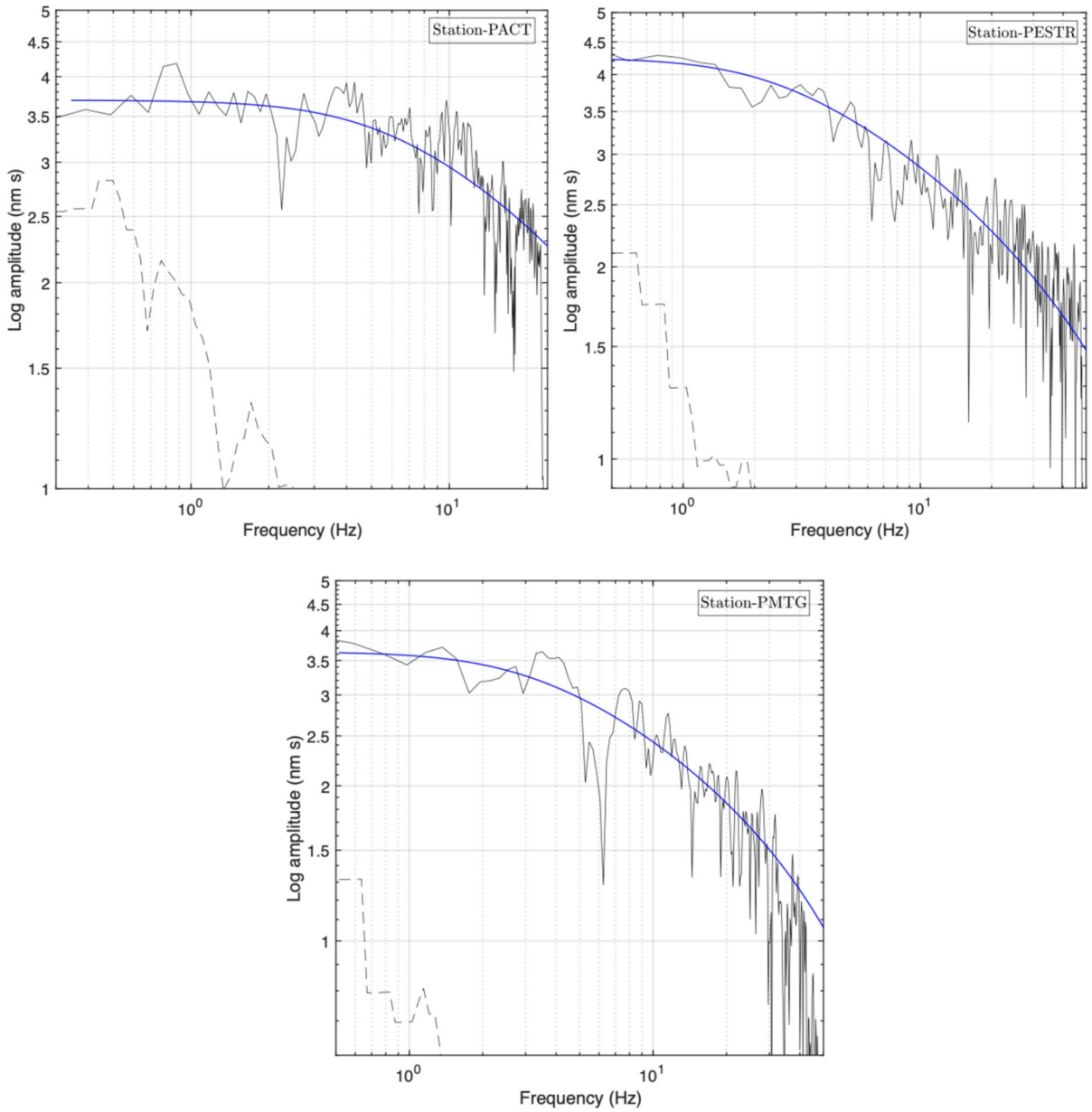

Fig. 4 Illustration of some displacement spectra obtained from P-waves, for the mainshock (M_L 4.9) on January 15, 2018. The black lines represent the observed source spectra for the vertical components of the three seismic stations; the solid blue lines represent the theoretical best-fit Brune spectra; and the dashed lines represent the noise spectra

The calculated values of the seismic moment (M_0), the moment magnitude (M_w), the corner frequency (f_c), the source radius (r_0) and the associated stress drop of the 82 local earthquakes are presented in Table 2 (in the appendix), with their respective uncertainties (standard deviation errors).

4.2 Discussion

Numerous studies have established empirical formulas that correlate moment magnitude scales with local magnitudes. In Fig. 6, we compare the local magnitude (M_L) values determined by Wachilala et al. (2023) with

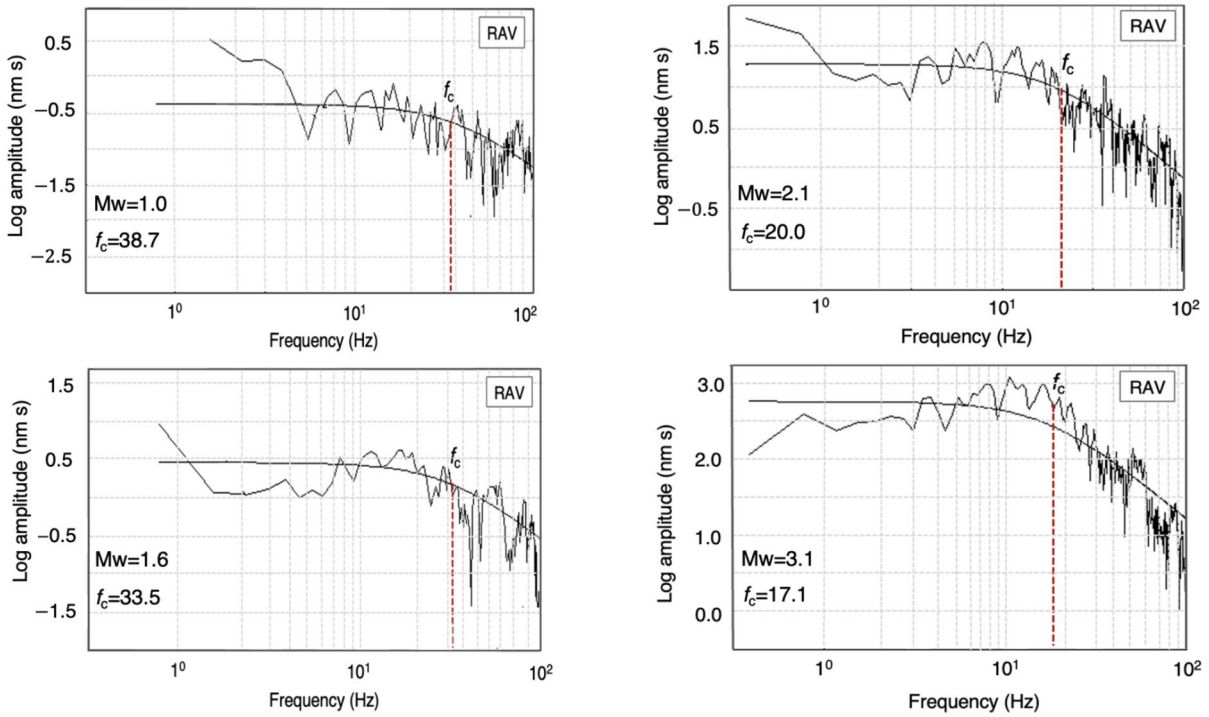

Fig. 5 Examples of displacement spectra obtained from one station for four earthquakes of different magnitudes, with the respective moment magnitudes and corner frequencies determined, illustrating the variation of f_c for M_w. The dashed red lines represent the corner frequency

the moment magnitudes (M_w) calculated in this study on the basis of Eq. (7). As expected, and in line with Kanamori and Anderson (1975), the M_L values are linearly related to M_w. Using our dataset, we derived the following relationship between the two magnitudes, the local magnitude (M_L) and the moment magnitude (M_w) (Fig. 6):

$$M_w = 0.71M_L + 0.55 \quad (7)$$

The slope is 0.71, and the correlation coefficient is 0.94. The comparison between M_L and M_w shows good correspondence within the analysed magnitudes ($0.6 \leq M_L \leq 4.9$). These results agree with the relationship proposed by Havskov et al. (2003), who estimated an M_L/M_w ratio of 2/3 for Norway; Moratto et al. (2017), who derived a scaling relationship between M_L and M_w for northeastern Italy; and Allen et al. (2004), who conducted a study in southeastern Australia. Several studies (e.g., Deichmann 2006; Moratto et al. 2017; Allen et al. 2004) have demonstrated that deviations between Mw and M_L values may be attributed to various physical factors, such as stress drops, rupture velocities, source complexities and rupture, radiation patterns, and rupture directivity.

We aim to analyse how the source radius (r_0) varies with the seismic moment (M_0). Figure 7 presents a graph with a logarithmic scale that shows the relationship between r_0 and M_0 for the set of seismic events included in this study. The diagonal lines on the graph that intersect the axes of the source radius and seismic moment represent constant stress drop values of 0.1, 1, 10 and 100 bars, respectively. Our analysis reveals that the logarithms of the seismic moments ($\log(M_0)$) range from 10.4 to 15.6 Nm, whereas the source radius (r_0) varies between 31.5 and 775.9 m.

Furthermore, approximately 80% of the events are limited to a stress drop range of 0.1 to 10 bars, whereas the remaining 20% values fall within the 10 to 100 bar range. On the other hand, as expected, we observed a tendency for the source radii to generally increase with increasing seismic moment. The source radius dimensions (31.5 m to 775.9 m) for

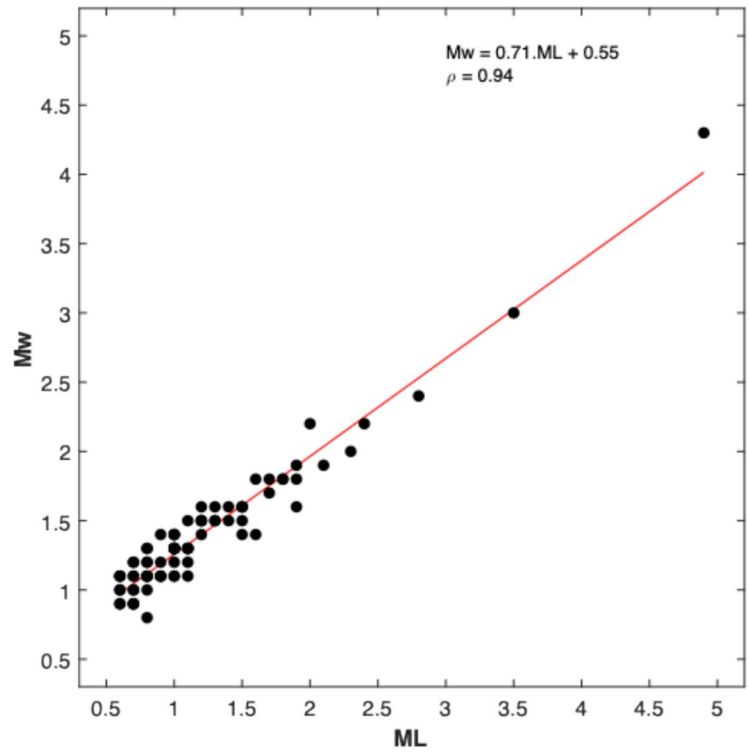

Fig. 6 Relationships between local (M_L) and moment (M_w) magnitudes. The best fit by least-squares regression (solid line) is also shown. where ρ represents the correlation coefficient

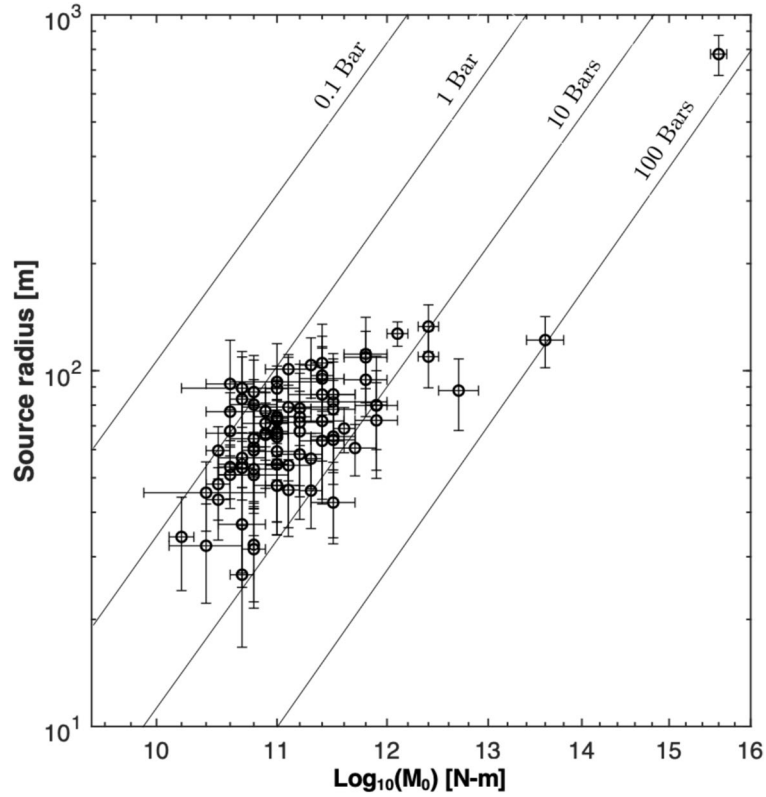

Fig. 7 Relationships between the source radius (r_0) and seismic moment (M_0), with their corresponding error bars. The lines are the stress drop constants

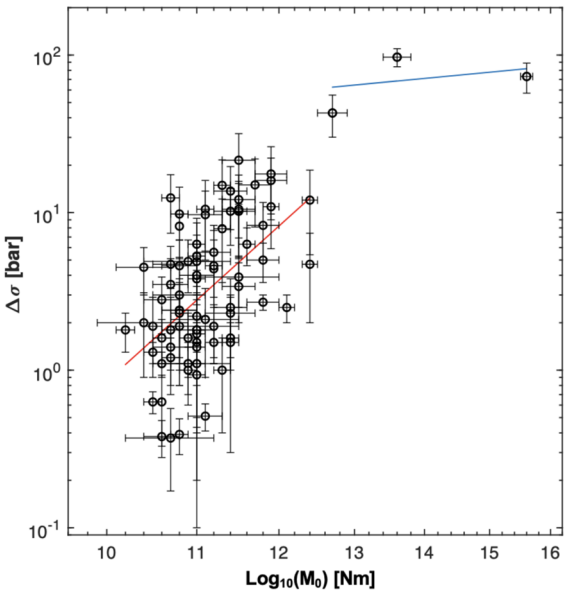

Fig. 8 Relationships between the stress drop (Δσ) and seismic moment (M_0), with their corresponding error bars. The circles indicate seismic events. The red regression line defines the first line segment for events with ($Log_{10}(M_0) \leq 12.5$): $Log_{10}(\Delta\sigma) = 0.480x + -4.837$. The correlation coefficient is 0.51. R-squared is 0.26. The blue regression line defines the second line segment for events with ($Log_{10}(M_0) > 12.5$): $Log10(\Delta\sigma) = 0.056x + 1.041$. The correlation coefficient is 0.46. R-squared is 0.22

the estimated seismic moments of the study region (Arraiolos seismic zone) suggest an intraplate type behaviour, how comproved the results of other studies of low-magnitude earthquakes in intraplate regions (e.g., Jiménez et al. 2015; Radulian et al. 2014; Moratto et al. 2019).

The stress drop is a critical source parameter for understanding the physical mechanisms underlying the generation of earthquakes. Figure 8 illustrates the variations in the stress drop (Δσ) and the seismic moment (M_0), which reflect the varying stresses of the seismic sources. We found that the three events with the highest seismic moment values ($\log_{10} M_0 > 12.5$) correspond to high stress drop values, resulting in nonlinear relationships with the smaller events ($\log_{10} M_0 \leq 12.5$). For this reason, we applied a segmented linear fit. The two groups of events can be associated with two levels of stress drops: one group, with an average of approximately 4 ± 6 bar, corresponds to the smaller events, while the other group with an average of approximately 60 ± 25 bar, corresponds to the larger events. However, there are several factors that can influence the observed behaviour:

(i) The difficulty in estimating the corner frequency for earthquakes of lower magnitude;
(ii) The complexity of the fault geometry or blockages in the fault segments;
(iii) Local geological properties may play an important role in the stress drop behaviour in our study region.

It is also important to note that larger magnitude earthquakes may have more efficient rupture propagation mechanisms (Kanamori and Brodsky 2004).

In general terms, the stress drop values (Δσ) varied from 0.4 to 97.0 bars (with an average of 7.3 bars), corresponding to seismic moment variations of $2.5 \times 10^{10} - 4.0 \times 10^{15}$ Nm. The stress drop estimates from this study can be compared with stress drops obtained by several authors in other intraplate regions. For example, the stress drops found by Jiménez et al. (2015) in northern Spain range from 0.006 to 29.462 MPa, with an average value of 1.076 MPa, with magnitudes ranging from 1.2 to 5.2. Franceschina et al. (2006) in the northeastern region of Italy, with events of magnitudes ranging from 2.0 to 5.7, reported stress drop values in the range of 0.07 to 5.31 MPa, with an average value of 0.73 MPa. Süle and Wéber (2013) in Hungary, with events of magnitudes ranging from 0.8 to 4.5, reported stress drop values in the range of 0.14 to 32.4 bars. Alloncle et al. (2025) in northwestern France obtained values in the range of 5.4 to 9.4 MPa for the largest magnitude earthquake ($M = 5.0$) in their dataset (M 1.7 to 5.0). However, to estimate the accuracy of the stress drop is not an easy task, since, being proportional to the cube of the corner frequency, the related uncertainty is tripled (Moratto et al. 2019). Several studies have explained the possible causes of such high uncertainties (e.g., Prieto et al. 2007; Kane et al. 2011; Abercrombie 2015; Kaneko and Shearer 2015). An error of 30% (Kane et al. 2011) or 50% in the stress drop estimation (Prieto et al. 2007) can be expected.

Figure 9 shows the variation in the stress drop with focal depth. Most events occurred mainly within the depth range of 12–13 km, resulting in a wide range of stress drop values, from 0.4 to 97.0 bars. It is important to note that the location of seismic sources is subject to some degree of uncertainty

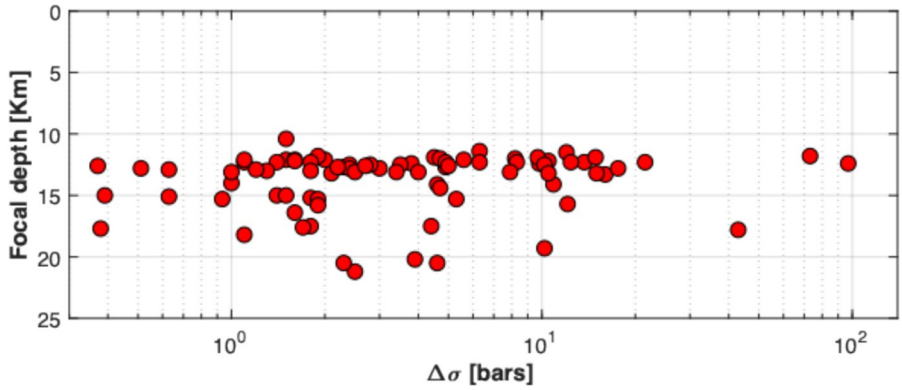

Fig. 9 Illustration of the depth distribution of the stress drop values (in bars). The red circles indicate seismic events

(Bondár and McLaughlin 2009; Kane et al. 2011). For this study, the uncertainties associated with the hypocentral location of the events vary range from approximatly 0.4 to 3 km. The clusters in the Aldeia da Serra zone (main seismic zone of Arraiolos), which constitute more than 70% of the events and are primarly concentrated at depth 12 to 13 km, with lower associated uncertainty (less than 2 km). In contrast, below 14 km depth, no clear trend of increasing or decreasing stress drop is observed.

In the present study, we aimed to establish a scaling relationship between the seismic moment and the corner frequency for the study region. Aki (1967) proposed that earthquakes are geometrically similar regardless of their size and that the interdependence of source parameters can be described by a scaling relationship. According to Aki (1967), the seismic moment varies with the cube root of the corner frequency. The relationship can be expressed as:

$$M_o \propto f_c^{-3} \tag{8}$$

This relationship implies that the stress drop is constant and does not depend on the magnitude of the earthquake. However, Izutani and Kanamori (2001) and Kanamori and Rivera (2004) proposed a modification to this scaling relationship, which can be expressed as

$$M_0 \sim f_c^{-3+\varepsilon} \tag{9}$$

where ε is a constant ≤ 1 that denotes the dependence of the stress drop or rupture velocity on the size of the seismic event.

Figure 10 illustrates the scaling relationship between the corner frequency (f_c) and seismic moment

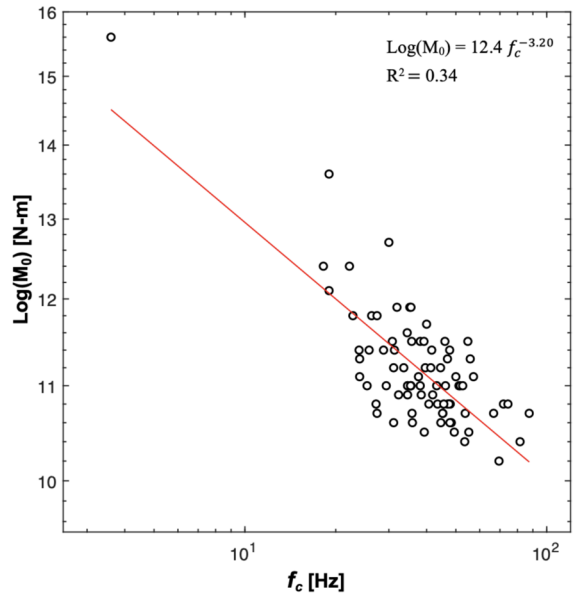

Fig. 10 Corner frequency (f_c) versus seismic moment (M_0) graph. The circles indicate seismic events. The red line is the best fit

(M_0) for the study region. The seismic moment decreases as the corner frequency increases, which is consistent with Aki's (1967) postulate. The corner frequency (f_c) is inversely related to the seismic source duration and reflects the dynamics of fault rupture and typically decreases as the seismic source size increases.

Using Eqs. (8) and (9), we derived the following relationship for the study region: $\mathrm{Log}(M_0) = 12.07\ f_c^{-3.20}$, where the estimated value of the scaling exponent $f_c^{-3+\varepsilon}$ was $\varepsilon = 0.20$. Several studies have investigated the scaling relationship between the

seismic moment and corner frequency. For example, Franceschina et al. (2006) analysed the source parameters of 53 local earthquakes of low to moderate magnitude ($2.0 < M_L < 5.7$) in the Friuli–Venezia Giulia area (northeastern Italy) and obtained a scaling relationship of $M_0 \propto f_c^{-3.43}$. Similarly, Rai et al. (2024) used 80 events ($1.5 < M_L < 3.5$) from the Siang region of the Arunachal Himalayas and derived a scaling relationship of $M_0 \propto f_c^{-3.18}$. Kumar et al. (2013), for events with magnitudes ranging from $0.7 \leq M_w \leq 3.7$, obtained a scaling relationship of $M_0 \propto f_c^{-3.34}$. Finally, Kanamori and Rivera (2004) reported that small and large earthquakes can exhibit significantly different stress drops and rupture velocities. These differences have critical implications for understanding the physics of fault rupture processes.

5 Conclusions

In the present study, we estimate the various parameters that characterize seismic sources that are determined through the spectral analysis of P-waves obtained from 82 local seismic events ($0.6 \leq M_L \leq 4.9$) that occurred in the Arraiolos area and surrounding areas following the Arraiolos earthquake of January 15, 2018. As expected, an increase in the source dimension is observed as the seismic moment increases. The source radii size (ranging from 31.5 to 775.9 m) suggest an intraplate regime. This indication is in line with other studies of low magnitude earthquakes conducted by several authors in other intraplate regions (e.g., Jiménez et al. 2015; Radulian et al. 2014; Alloncle et al. 2025). We found a large variation of stress drop (ranging from 0.4 to 97.0 bars) for earthquakes of different magnitudes in the same tectonic environment. We found a large variation of stress drop (ranging from 0.4 to 97.0 bars) for earthquakes of different magnitudes in the same tectonic environment. On the other hand, the results indicate that stress drop and seismic moment do not have a linear correlation. Two groups of events can be identified: a low-stress-drop group for smaller earthquakes ($\log_{10}(M_0) \leq 12.5$) in the order of approximately 4 bar, and the high-stress-drop case for larger earthquakes ($\log_{10}(M_0) > 12.5$) in the order of approximately 60 bar. This behaviour may be influenced by uncertainties in the estimates of corner frequencies for smaller earthquakes. However, the complexity of the fault geometry or blockages in the fault segments, and variation in local geological properties may play an important role in the stress drop behaviour in our study region. Most of the events studied are concentrated mainly at depths of 12 to 13 km, which constitutes the main focus of seismic rupture in the study area, recently confirmed by seismic tomography studies in this region, conducted by Hamak et al. (2025). The scaling relationship established between the seismic moment (M_0) and the corner frequency (f_c) for the study area is as follows: $\mathrm{Log}(M_0) = 12.4\ f_c^{-3.20}$, which aligns with observations from other regions with similar characteristics. This scaling law has several implications for seismogenic regions. The empirical M_w–M_L relationships developed for local earthquakes are consistent and could be highly useful for investigating the dynamic processes in seismic sources, such as stress drops, rupture propagation velocity, and fault plane directivity. M_w estimates can also enhance seismic catalogues for the study area. The estimated source parameters and their scaling relationships are valuable tools for understanding and assessing seismic hazard in a region.

Appendix

Table 1 Details of the earthquake parameters determined by Wachilala et al. (2023) and used in this study

Event Nº	Date and Time (yy/mm/dd hh:mm:ss)	Latitude (° N)	Longitude (° W)	Depth (km)	RMS	M_L
1	2018/01/15 11:51:40.00	38.783	7.949	11.8	0.3	4.9
2	2018/01/15 18:59:36.00	38.741	7.859	17.5	0.3	1.6
3	2018/01/15 19:47:52.30	38.785	7.965	11.4	0.3	1.7
4	2018/01/16 01:51:58.30	38.785	7.958	10.4	0.2	1.1
5	2018/01/16 02:04:59.20	38.775	7.961	11.5	0.2	2.0
6	2018/01/16 18:28:41.20	38.788	7.979	12.9	0.0	0.6
7	2018/01/17 19:48:40.30	38.786	7.970	12.4	0.1	0.9
8	2018/01/17 22:32:56.20	38.781	7.970	12.1	0.1	1.0
9	2018/01/18 06:55:30.90	38.785	7.966	12.8	0.1	1.1
10	2018/01/19 08:31:38.10	38.784	7.989	13.2	0.1	0.9
11	2018/01/20 22:03:11.60	38.787	7.959	12.5	0.1	0.6
12	2018/01/23 01:56:47.70	38.778	7.973	12.3	0.1	1.5
13	2018/01/24 12:58:51.00	38.781	7.971	12.3	0.1	1.5
14	2018/01/24 21:35:44.80	38.786	7.971	12.0	0.1	0.8
15	2018/01/25 17:25:28.50	38.780	7.975	11.9	0.1	0.7
16	2018/01/26 02:45:55.10	38.777	7.970	12.4	0.1	0.9
17	2018/01/26 03:27:27.70	38.724	7.923	15.3	0.1	1.1
18	2018/01/26 08:58:32.90	38.774	7.970	12.2	0.1	1.0
19	2018/01/26 15:47:57.10	38.723	7.922	15.2	0.1	0.8
20	2018/01/27 01:32:33.10	38.866	7.704	17.7	0.1	0.8
21	2018/01/27 18:15:36.40	38.783	7.965	12.1	0.1	0.7
22	2018/01/28 20:36:40.20	38.783	7.968	12.3	0.1	0.8
23	2018/01/28 23:20:20.30	38.778	7.960	12.0	0.1	0.8
24	2018/01/30 13:41:32.60	38.725	7.923	15.1	0.1	0.7
25	2018/01/30 15:46:46.10	38.783	7.962	11.9	0.1	1.2
26	2018/02/01 04:15:42.10	38.775	7.970	12.4	0.1	3.5
27	2018/02/01 17:36:27.80	38.784	7.969	11.9	0.1	1.0
28	2018/02/02 22:45:20.60	38.775	7.973	12.3	0.1	1.0
29	2018/02/03 04:43:08.20	38.780	7.971	12.6	0.1	1.0
30	2018/02/04 16:47:49.80	38.779	7.973	12.1	0.1	1.3
31	2018/02/07 10:40:31.60	38.785	7.969	12.3	0.1	1.0
32	2018/02/07 17:42:23.70	38.783	7.963	11.8	0.1	0.6
33	2018/02/08 06:34:58.00	38.800	7.942	15.3	0.1	0.6
34	2018/02/09 03:10:24.20	38.773	7.974	12.7	0.1	1.1
35	2018/02/09 03:10:38.10	38.774	7.975	12.7	0.1	1.2
36	2018/02/12 03:35:39.30	38.825	7.989	21.2	0.1	2.3
37	2018/02/14 12:47:37.50	38.779	7.971	12.5	0.1	0.6
38	2018/02/19 05:51:46.50	38.779	7.972	12.5	0.1	0.6
39	2018/02/24 10:52:09.60	38.777	7.973	12.3	0.1	1.7
40	2018/02/25 00:27:45.60	38.787	7.967	12.3	0.1	1.0
41	2018/03/26 10:49:49.60	38.740	7.868	20.2	0.3	1.2
42	2018/03/29 13:29:14.10	38.789	7.977	13.3	0.1	1.9

Table 1 (continued)

Event Nº	Date and Time (yy/mm/dd hh:mm:ss)	Latitude (º N)	Longitude (º W)	Depth (km)	RMS	M_L
43	2018/03/29 21:46:01.40	38.795	7.987	19.3	0.1	1.4
44	2018/04/04 00:40:45.50	38.828	7.957	20.5	0.1	1.0
45	2018/04/14 21:38:51.10	38.791	7.972	14.1	0.2	1.0
46	2018/04/15 00:33:12.70	38.795	7.970	14.0	0.2	1.1
47	2018/04/16 00:28:13.30	38.789	7.927	12.3	0.1	0.8
48	2018/04/16 20:56:03.60	38.788	7.963	13.0	0.1	0.7
49	2018/04/19 18:37:39.60	38.766	7.988	12.3	0.2	0.8
50	2018/04/27 13:09:20.60	38.781	7.967	12.8	0.0	0.7
51	2018/04/27 15:33:53.40	38.780	7.969	12.5	0.0	1.3
52	2018/04/28 03:39:22.00	38.779	7.966	12.8	0.1	1.9
53	2018/04/28 19:20:11.80	38.723	7.897	17.5	0.1	0.8
54	2018/04/29 21:44:36.60	38.784	7.964	12.7	0.1	0.8
55	2018/05/01 17:30:51.10	38.726	7.918	16.4	0.1	0.7
56	2018/05/04 17:41:42.00	38.723	7.913	15.0	0.1	0.9
57	2018/05/09 04:15:02.80	38.722	7.893	18.2	0.1	0.6
58	2018/05/09 23:27:12.30	38.769	7.784	17.8	0.1	2.8
59	2018/05/10 14:36:13.10	38.723	7.896	14.1	0.3	2.1
60	2018/05/11 14:14:03.80	38.780	7.971	12.8	0.0	1.0
61	2018/05/12 10:43:00.40	38.822	7.991	20.5	0.0	1.0
62	2018/05/13 19:58:59.20	38.784	7.974	12.1	0.0	0.7
63	2018/05/13 20:14:10.60	38.788	7.971	13.1	0.1	1.5
64	2018/05/13 20:16:47.70	38.784	7.974	12.1	0.0	1.2
65	2018/05/14 02:00:23.00	38.784	7.974	12.2	0.0	0.7
66	2018/05/26 02:24:25.40	38.727	7.894	17.6	0.1	1.1
67	2018/05/26 21:04:29.70	38.787	7.974	13.1	0.1	1.2
68	2018/05/29 19:48:56.60	38.723	7.918	15.8	0.1	1.5
69	2018/05/29 21:38:29.70	38.726	7.916	15.3	0.0	1.1
70	2018/05/31 02:41:37.20	38.781	7.992	13.2	0.1	1.6
71	2018/05/31 02:50:15.50	38.785	7.995	13.0	0.0	1.0
72	2018/05/31 07:57:37.40	38.785	7.995	13.1	0.0	1.0
73	2018/06/01 02:40:32.90	38.781	7.991	13.2	0.1	1.4
74	2018/06/01 21:04:33.70	38.781	7.973	13.1	0.1	1.5
75	2018/06/03 01:29:42.60	38.785	7.996	13.1	0.0	0.8
76	2018/06/03 21:00:18.70	38.779	7.972	12.6	0.1	1.8
77	2018/06/03 21:00:50.90	38.780	7.973	12.6	0.1	1.8
78	2018/06/04 06:59:39.10	38.784	7.996	12.9	0.0	0.7
79	2018/06/11 06:11:08.10	38.727	7.917	15.0	0.0	0.9
80	2018/06/11 21:47:11.20	38.722	7.924	15.7	0.1	1.9
81	2018/06/27 03:24:22.50	38.531	8.249	14.4	0.3	2.4
82	2018/06/27 05:17:28.10	38.533	8.258	15.0	0.3	1.3

Table 2 Source parameters estimated from the P-wave spectra

Event N°	Date (yy/mm/dd)	f_c(Hz)	***SD*** f_c	M_0 *(Nm)*	SD M_0	M_w	**SD** $\mathbf{M_w}$	r_0(m)	SDr_0	Δ_σ(bar)	**SD**Δ_σ
1	2018/01/15	3.6	1.5	15.6	0.1	4.3	0.1	775.9	0.10	73.1	15.8
2	2018/01/15	39.6	7.1	11.2	0.0	1.4	0.0	67.5	0.02	4.4	3.3
3	2018/01/15	34.5	5.0	11.6	0.1	1.7	0.0	68.8	0.01	6.3	1.7
4	2018/01/16	35.5	5.0	11.0	0.0	1.3	0.0	65.1	0.01	1.5	0.0
5	2018/01/16	22.2	4.5	12.4	0.1	2.2	0.0	109.5	0.02	12.0	6.6
6	2018/01/16	39.3	1.0	10.5	0.1	0.9	0.1	59.6	0.01	0.6	0.1
7	2018/01/17	46.2	5.6	11.0	0.1	1.2	0.0	54.6	0.02	3.8	1.7
8	2018/01/17	31.1	6.4	11.2	0.1	1.4	0.1	78.3	0.02	1.5	0.4
9	2018/01/18	47.0	7.2	10.8	0.3	1.1	0.2	50.9	0.01	3.0	2.2
10	2018/01/19	37.6	5.8	11.1	0.4	1.4	0.2	79.0	0.03	2.1	1.2
11	2018/01/20	53.7	9.7	10.7	0.2	1.1	0.1	54.6	0.03	3.5	1.6
12	2018/01/23	47.7	8.8	11.4	0.2	1.5	0.1	72.2	0.03	13.7	5.9
13	2018/01/24	54.8	0.9	11.5	0.2	1.6	0.2	42.6	0.01	21.5	10.2
14	2018/01/24	71.9	10.0	10.8	0.0	1.1	0.1	32.4	0.01	8.2	1.5
15	2018/01/25	81.6	10.4	10.4	0.3	0.9	0.2	32.2	0.01	4.5	1.5
16	2018/01/26	74.4	5.1	10.8	0.1	1.1	0.1	31.5	0.01	9.8	4.7
17	2018/01/26	29.4	7.6	11.0	0.1	1.3	0.1	89.1	0.03	0.9	0.5
18	2018/01/26	57.2	9.4	11.1	0.1	1.3	0.1	46.2	0.01	10.5	5.5
19	2018/01/26	69.5	10	10.2	0.1	0.8	0.1	34.1	0.01	1.8	0.5
20	2018/01/27	31.1	1.9	10.6	0.2	1.0	0.1	76.7	0.01	0.4	0.1
21	2018/01/27	53.5	6.7	10.4	0.5	0.9	0.2	45.4	0.01	2.0	1.1
22	2018/01/28	87.5	10.0	10.7	0.1	1.1	0.1	26.7	0.01	12.4	5.0
23	2018/01/28	66.7	9.7	10.7	0.2	1.1	0.1	37.0	0.01	4.7	1.4
24	2018/01/30	35.9	5.6	10.6	0.0	1.0	0.0	67.6	0.01	0.6	0.3
25	2018/01/30	55.8	8.1	11.3	0.1	1.5	0.1	46.0	0.01	14.9	6.7
26	2018/02/01	19.9	3.7	13.6	0.2	3.0	0.1	121.9	0.02	97.0	12.7
27	2018/02/01	50.0	8.6	11.1	0.2	1.4	0.1	54.2	0.02	9.7	4.0
28	2018/02/02	25.4	2.8	11.0	0.4	1.3	0.2	93.0	0.01	1.1	0.9
29	2018/02/03	27.4	5.8	10.7	0.5	1.1	0.3	89.3	0.02	0.4	0.2
30	2018/02/04	23.9	6.4	11.4	0.1	1.5	0.1	105.1	0.03	1.6	1.3
31	2018/02/07	51.2	7.1	11.0	0.1	1.3	0.1	47.5	0.01	6.3	2.9
32	2018/02/07	40.7	9.8	10.8	0.1	1.1	0.1	61.0	0.02	1.9	1.1

Table 2 (continued)

Event N°	Date (yy/mm/dd)	f_c(Hz)	***SD*** f_c	M_0 *(Nm)*	SD M_0	M_w	**SD** $\mathbf{M_w}$	r_0(m)	***SD***r_0	Δ_σ(bar)	**SD**Δ_σ
33	2018/02/08	55.2	5.7	10.5	0.1	0.9	0.1	43.4	0.01	1.9	1.0
34	2018/02/09	41.9	9.2	10.9	0.5	1.2	0.3	66.7	0.02	4.9	1.8
35	2018/02/09	31.3	8.2	11.4	0.3	1.5	0.2	85.7	0.03	2.3	0.7
36	2018/02/12	19.0	1.8	12.1	0.1	2.0	0.1	127.1	0.01	2.5	0.5
37	2018/02/14	43.5	7.0	10.8	0.2	1.1	0.1	80.3	0.03	2.4	1.2
38	2018/02/19	48.3	7.2	10.6	0.2	1.0	0.1	91.8	0.03	2.8	1.1
39	2018/02/24	26.3	6.6	11.8	0.2	1.8	0.2	111.3	0.03	8.3	3.3
40	2018/02/25	34.6	5.1	11.0	0.1	1.3	0.1	67.5	0.01	1.4	0.1
41	2018/03/26	35.7	8.9	11.5	0.5	1.6	0.3	81.7	0.03	3.9	1.4
42	2018/03/29	35.2	6.3	11.9	0.2	1.9	0.1	72.5	0.02	16.0	6.2
43	2018/03/29	41.6	6.5	11.4	0.2	1.5	0.1	63.5	0.02	10.2	4.0
44	2018/04/04	47.9	5.8	10.8	0.2	1.2	0.1	52.9	0.01	4.6	2.1
45	2018/04/14	41.3	6.7	11.2	0.1	1.4	0.1	74.2	0.03	4.6	2.1
46	2018/04/15	24.0	5.8	11.3	0.1	1.5	0.1	103.7	0.02	1.0	0.6
47	2018/04/16	34.6	7.4	11.0	0.1	1.3	0.1	72.4	0.01	1.8	1.3
48	2018/04/16	49.4	5.3	10.5	0.1	0.9	0.0	48.0	0.01	1.3	0.2
49	2018/04/19	51.7	5.2	11.0	0.2	1.3	0.1	47.6	0.01	4.9	2.3
50	2018/04/27	47.5	6.0	10.8	0.2	1.1	0.1	64.4	0.03	2.4	1.4
51	2018/04/27	38.1	7.7	11.5	0.2	1.6	0.2	77.9	0.03	10.2	5.1
52	2018/04/28	35.5	6.6	11.9	0.2	1.8	0.1	79.8	0.03	17.6	8.6
53	2018/04/28	45.3	5.6	10.7	0.1	1.1	0.1	53.3	0.01	1.8	1.1
54	2018/04/29	38.1	5.9	11.0	0.1	1.2	0.1	66.4	0.01	2.2	2.1
55	2018/05/01	47.8	7.8	10.6	0.1	1.0	0.0	51.0	0.01	1.6	0.5
56	2018/05/04	45.2	6.7	10.7	0.2	1.1	0.1	56.9	0.01	1.4	0.4
57	2018/05/09	44.6	2.0	10.6	0.1	1.0	0.0	53.6	0.01	1.1	0.2
58	2018/05/09	30.0	5.3	12.7	0.2	2.4	0.2	87.9	0.02	42.9	12.8
59	2018/05/10	31.9	7.7	11.9	0.1	1.9	0.1	80.0	0.02	10.9	5.0
60	2018/05/11	24.0	4.2	11.1	0.2	1.3	0.1	101.0	0.01	0.5	0.1
61	2018/05/12	45.6	7.3	10.8	0.1	1.1	0.1	59.7	0.02	2.3	1.2
62	2018/05/13	34.6	6.4	10.9	0.2	1.2	0.1	71.1	0.01	1.1	0.4
63	2018/05/13	30.8	7.2	11.5	0.2	1.6	0.2	85.8	0.02	3.4	1.4
64	2018/05/13	44.5	8.3	11.2	0.2	1.4	0.1	58.2	0.02	5.6	2.7

Table 2 (continued)

Event N°	Date (yy/mm/dd)	f_c(Hz)	***SD*** f_c	M_0 *(Nm)*	SD M_0	M_w	**SD** $\mathbf{M_w}$	r_0(m)	***SD*** r_0	Δ_σ(bar)	**SD** Δ_σ
65	2018/05/14	38.4	8.7	10.9	0.1	1.2	0.1	66.0	0.01	1.6	0.7
66	2018/05/26	35.5	8.5	11.0	0.1	1.3	0.0	73.5	0.02	1.7	1.3
67	2018/05/26	46.9	9.3	11.3	0.1	1.5	0.1	56.6	0.01	7.9	4.3
68	2018/05/29	33.6	4.2	11.2	0.3	1.4	0.2	71.6	0.01	1.9	0.7
69	2018/05/29	52.7	9.0	11.0	0.1	1.3	0.1	54.5	0.02	5.3	3.3
70	2018/05/31	40.0	7.5	11.7	0.2	1.8	0.1	60.6	0.01	15.0	6.9
71	2018/05/31	35.4	8.8	11.0	0.2	1.3	0.1	74.2	0.02	1.8	1.0
72	2018/05/31	43.2	8.9	11.0	0.2	1.3	0.1	59.3	0.01	4.0	2.3
73	2018/06/01	39.2	7.0	11.5	0.2	1.6	0.1	65.3	0.01	10.5	5.3
74	2018/06/01	28.8	6.6	11.4	0.2	1.6	0.1	95.0	0.03	2.5	1.3
75	2018/06/03	32.3	5.8	10.9	0.1	1.2	0.1	77.0	0.01	1.0	0.4
76	2018/06/03	27.4	4.9	11.8	0.2	1.8	0.1	94.3	0.02	5.0	1.4
77	2018/06/03	22.8	2.4	11.8	0.2	1.8	0.1	109.0	0.02	2.7	0.3
78	2018/06/04	35.8	5.5	10.7	0.1	1.1	0.1	83.2	0.03	1.2	0.4
79	2018/06/11	27.2	3.0	10.8	0.1	1.1	0.1	87.1	0.02	0.4	0.1
80	2018/06/11	46.0	4.7	11.5	0.2	1.6	0.1	63.9	0.03	12.1	5.2
81	2018/06/27	18.2	2.8	12.4	0.1	2.2	0.1	133.1	0.02	6.3	2.7
82	2018/06/27	25.8	2.6	11.4	0.1	1.5	0.1	96.9	0.02	1.5	0.5

$f_c(Hz)$– is the corner frequency;$M_0(Nm)$– is the seismic moment (unit Newton-metre);M_w– Moment magnitude;$r_0(m)$– is the source radius in metre;$\Delta_\sigma(bar)$– is the stress drop in bars. SD is the standard deviation for f_c, M_0, Mw,r_0, andΔ_σ

Acknowledgements The authors would like to thank the Center for SCI-TECH Research in Earth System and Energy (CREATE) of the University of Évora, Portugal, for all the support needed to carry out this research. We are also thankful for the support of the Higher Institute of Education Sciences of Huíla (ISCED-Huíla), Angola. This work is funded by national resources through the FCT—Fundação para a Ciência e Tecnologia, I.P., in the framework of the ICT project with the references UIDB/04683/2020 and UIDP/04683/2020. We are also thankful for the partnership with IPMA (Instituto Português do Mar e da Atmosfera). Our sincere thanks to the editor Angela Saraò and the three anonymous reviewers for their fruitful comments and appropriate suggestions, which helped us to improve the manuscript.

Author contributions P.W. Conceptualization, methodology, validation, formal analysis, research, data curation, writing – original draft preparation, writing – review and editing. J.B. formal analysis, validation, overall supervision, writing – review and editing. B.C and M.B. formal analysis, general review and editing of the manuscript. All authors reviewed the manuscript.

Funding Open access funding provided by FCT|FCCN (b-on).

Data availability Information on the Arraiolos seismic network (code 7N) can be found at https://doi.org/10.7914/SN/7N_2018. Additional data were provided by the Instituto Português do Mar e da Atmosfera (IPMA) and are available upon request at http://ceida.ipma.pt. The raw data supporting further work based on this study will be made available by the authors.

Declarations

Conflict of interest The authors declare no competing interests.

References

Abercrombie RE (2015) Investigating uncertainties in empirical Green's function analysis of earthquake source parameters. J Geophys Res Solid Earth 120:4263–4277. https://doi.org/10.1002/2015JB011984

Aki K (1967) Scaling law of seismic spectrum. J Geophys Res 72:1217–1231

Aki K, Richards PG (1980) Quantitative seismology. Theory and Methods. Vol. I and II. W. H. Freeman and Co., San Francisco, p 932

Allen TI, Gibson G, Brown A, Cull JP (2004) Depth variation of seismic source scaling relations: implications for earthquake hazard in southeastern Australia. Tectonophysics 390:5–24. https://doi.org/10.1016/j.tecto.2004.03.018

Allmann BP, Shearer PM (2009) Global variations of stress drop for moderate to large earthquakes. J Geophys Res 114:B01310. https://doi.org/10.1029/2008JB005821

Alloncle M, Bonnin M, Mocquet A (2025) Earthquake Source Spectra and Site Attenuation in Northwestern France. Bull Seismol Soc Am. https://doi.org/10.1785/0120240122

Anderson DL, Ben-Menahem A, Archambeau CB (1965) Attenuation of Seismic Energy in the Upper Mantle. J Geophys Res 70(6):1441–1448

Aptekman Zh, Daragan S, Dolgopolov O, Zakharova A, Zobin V, Kogan S, Korchagina O, Moskvina A, Polikarpova L, Chepkunas L (1988) Use of P-Wave Spectra to Determine Earthquake Source Parameters: Standardization of Raw Data and Calculation of Amplitude Spectra. J Volcanol Seismol 7:235–251

Araujo A, Caldeira B, Martins A, Borges JF, Moreira N, Araújo JF, Maia M, Vicente S, Afonso P, Espanhol D et al (2020) Macrossismicidade associada ao sismo de Arraiolos do dia 15 de janeiro de 2018 com M=4,9 e eventuais implicações na geometria da rutura. Comunicações Geológicas 107:35–37 (in Portuguese)

Araújo A, Matos C, Martins A (2010) The Aldeia da Serra hill (Arraiolos): an active "Push up" associated with the Ciborro fault and the S. Gregório lineament? Revista Electrónica de Ciências da Terra Geosciences On-line Journal 11(10):1645-0388. VIII Congresso Nacional de Geologia. (in Portuguese)

Argus DF, Gordon RG, DeMets C, Stein S (1989) Closure of the Africa-Eurasia-North America Plate motion circuit and tectonics of the Gloria Fault. J Geophys Res Atmos 94:5585–5602

Attanayake J, Ferreira A, Berbellini A, Morelli A (2017) Crustal structure beneath Portugal from teleseismic Rayleigh Wave Ellipticity. Tectonophys 712–713:344–361

Baumbach M, Bormann P (2012) Determination of source parameters from seismic spectra. - In: Bormann, P. (Ed.), New Manual of Seismological Observatory Practice 2 (NMSOP-2), Potsdam: Deutsches GeoForschungsZentrum GFZ, 1–7. https://doi.org/10.2312/GFZ.NMSOP-2_EX_3.4

Bezzeghoud M, Adam C, Buforn E, Borges J, Caldeira B (2014) Seismicity along the Azores-Gibraltar region and global plate kinematics. J Seismol 18:205–220. https://doi.org/10.1007/s10950-013-9416-x

Bezzeghoud M, Borges JF, Caldeira B (2012) Fontes sísmicas ao longo da fronteira de placas tectónicas entre os Açores e a Argélia: um modelo sismotectónico. In: Dias R, Araújo A, Terrinha P, Kullberg JC (eds) Geologia de Portugal. Escolar Editora 2:747–790

Bondár I, McLaughlin KL (2009) A New Ground Truth Data Set For Seismic Studies. Seismol Res Lett 80:465–472. https://doi.org/10.1785/gssrl.80.3.465

Borges JF, Fitas AJ, Bezzeghoud M, Teves-Costa P (2001) Seismotectonics of Portugal and its adjacent Atlantic area. Tectonophysics 331:373–387

Brune JN (1970) Tectonic stress and the spectra of seismic shear waves from earthquakes. J Geophys Res 75:4997–5009

Brune JN (1971) Correction: tectonic stress and the spectra of seismic shear waves from earthquakes. J Geophys Res 76:5002

Carvalhosa A (1999) Carta Geológica de Portugal na Escala 1/50.000. Nota Explicativa da Folha 36–C Arraiolos. 1ª Edição, Instituto Geológico e Mineiro. Lisboa, Portugal, p 52

Carvalhosa A, Zbyszewski G (1994) Carta Geológica de Portugal na Escala 1/50.000. Nota Explicativa da Folha 35–D Montemor-O-Novo. 1ª Edição, Instituto Geológico e Mineiro. Lisboa, Portugal, p 86

Deichmann N (2006) Local Magnitude, a Moment Revisited. Bull Seism Soc Am 96(4A):1267–1277

DeMets C, Gordon RG, Argus DF (2010) Geologically current plate motions. Geophys J Int 181:1–80. https://doi.org/10.1111/j.1365-246X.2009.04491.x

Denolle MA, Shearer PM (2016) New perspectives onself-similarity for shallow thrust earthquakes. J Geophys Res Sol Earth 121:6533–6565

Fontiela J, Bezzeghoud M (2018) Arraiolos [Data set]. International Federation of Digital Seismograph Networks. https://doi.org/10.7914/SN/7N_2018

Franceschina G, Kravanja S, Bressan G (2006) Source parameters and scaling relationships in the Friuli-Venezia Giulia (Northeastern Italy) region. Phys Earth Planet Inter 154:148–167

Goebel THW, Hauksson E, Shearer PM, Ampuero JP (2015) Stress-drop heterogeneity within tectonically complex regions: a case study of San Gorgonio Pass, southern California. Geophys J Int 202:514–528

Hamak I, Wachilala P, Borges J, Koulakov I, Araújo A, Bezzeghoud M (2025) Local Seismic Tomography Reveals the Crustal Structure Beneath Arraiolos (Central Portugal): Earthquake of ML 4.9 (15 January 2018). Seismol Res Lett XX, 1–19. https://doi.org/10.1785/0220240409.

Hanks TC, Wyss M (1972) The use of body-wave spectra in the determination of seismic-source parameters. Bull Seismol Soc Am 62:561–589

Hanks TC, Kanamori H (1979) A Moment Magnitude Scale. J Geophys Res 84:2348–2350

Haskell NA (1964) Total energy and energy spectral density of elastic wave radiation from propagating faults. Bull Seismol Soc Am 54(6A):1811–1841

Havskov J, Ottemoeller L (2010) Routine data processing in earthquake seismology. Springer, Dordrecht

Havskov J, Peña JA, Ibáñez JM, Ottemöller L, Martínez-Arévalo C (2003) Magnitude scales for very local earthquakes. Application for Deception Island Volcano (Antarctica). J Volcanology Geothermal Res 128:115-133. https://doi.org/10.1016/S0377-0273(03)00250-6

Izutani Y, Kanamori H (2001) Scale-dependence of seismic energy-to-moment ratio for strike-slip earthquakes in Japan. Geophys Res Lett 28:4007–4010

Jiménez A, García-García JM, Romacho MD, García-Jerez A, Luzón F (2015) Source Parameters of Earthquakes Recorded Near the Itoiz Dam (Northern Spain). Pure Appl Geophys 172:3163–3177. https://doi.org/10.1007/s00024-014-0883-y

Kanamori H (1977) The energy release in great earthquakes. J Geophys Res 82(20):2981–2987

Kanamori H (1983) Magnitude scale and quantification of earthquakes. Tectonophys 93:185–199

Kanamori H, Anderson DL (1975) Theoretical basis of some empirical relations in seismology. Bull Seismol Soc Am 65(5):1073–1095

Kanamori H, Brodsky EE (2004) The physics of earthquakes. Rep Prog Phys 67:1429–1496

Kanamori H, Rivera L (2004) Static and Dynamic Scaling Relations for Earthquake and Their Implications for Rupture Speed and Stress Drop. Bull Seismol Soc Am 94:314–319

Kane DL, Prieto GA, Vernon FL, Shearer PM (2011) Quantifying seismic source parameter uncertainties. Bull Seismol Soc Am 101:535–543. https://doi.org/10.1785/0120100166

Kaneko Y, Shearer PM (2015) Variability of seismic source spectra, estimated stress drop, and radiated energy, derived from cohesive-zone models of symmetrical and asymmetrical circular and elliptical ruptures. J Geophys Res Solid Earth 120:1053–1079. https://doi.org/10.1002/2014JB011642.Doi:10.1002/2014JB011642

Kumar A, Kumar A, Gupta SC, Mittal H, Kumar R (2013) Source parameters and fmax in Kameng region of Arunachal Lesser Himalaya. J Asian Earth Sc 70–71:35–44

Madariaga R (1978) The dynamic field of Haskell's rectangular dislocation fault model. Bull Seismol Soc Am 68(4):869–887

Mandal P, Dutta U (2011) Estimation of Earthquake Source Parameters in the Kachchh Seismic Zone, Gujarat, India, from Strong-Motion Network Data Using a Generalized Inversion Technique. Bull Seismol Soc Am 101(4):1719–1731

Maruyama T (1963) On the force equivalents of dynamical elastic dislocations with reference to the earthquake mechanism. Bull Earthq Res Inst 41(3):467–486

Modiano T, Hatzfeld D (1982) Experimental study of the spectral content for shallow earthquakes. Bull Seismol Soc Am 72:1739–1758

Moratto L, Romano MA, Laurenzano G, Colombelli S, Priolo E, Zollo A, Saraò A, Picozzi M (2019) Source parameter analysis of microearthquakes recorded around the underground gas storage in the Montello-Collalto Area (Southeastern Alps, Italy). Tectonophysics 762:159–168. https://doi.org/10.1016/j.tecto.2019.04.030

Moratto L, Saraò A, Priolo E (2017) Moment Magnitude (M_w) Estimation of Weak Seismicity in Northeastern Italy. Seismol Res Lett 88(6):1455–1464. https://doi.org/10.1785/0220170063

Natale G, Iannaccone G, Martini M et al (1987) Seismic sources and attenuation properties at the Campi Flegrei volcanic area. PAGEOPH 125:883–917

Ottemöller L, Havskov J (2003) Moment Magnitude Determination for Local and Regional Earthquakes Based on Source Spectra. Bull Seismol Soc Am 93(1):203–214

Ottemöller L, Voss PH, Havskov J (2016) SEISAN Earthquake analysis software for windows, solaris, linux and macosx, Version 10.5. University of Bergen, Bergen, Norway, p 465

Pereira MF, Chichorro M, Moita P, Santos JF, Solá AMR, Williams IS, Silva JB, Armstrong RA (2015) The multistage crystallization of zircon in calc-alkaline granitoids: U-Pb age constraints on the timing of Variscan tectonic activity in SW Iberia. Int J Earth Sci (Geol Rundsch) 104:1167–1183

Prieto GA, Thomson DJ, Vernon FL, Shearer PM, Parker RL (2007) Confidence intervals for earthquake source parameters. Geophys J Int 168:1227–1234. https://doi.org/10.1111/j.1365-246X.2006.03257.x

Pujades LG, Canas JÁ, Egozcue JJ, Puigvi MA, Gallart J, Lana X, Pous J, Casas A (1990) Coda Q distribution in the Iberian Peninsula. Geophys J Int 100:285–301

Radulian M, Popescu E, Borleanu F, Diaconescu M (2014) Source parameters of the December 2011–January 2012 earthquake sequence in Southern Carpathians, Romania. Tectonophys 623:23–38

Rai A, Mittal H, Singh GP (2024) Estimation of Source and Spectral Decay Parameters for Local Earthquakes in Siang Region of Arunachal Himalaya and Its Implication to the Tectonics and Crustal Heterogeneity. Pure Appl Geophys 181:789–813. https://doi.org/10.1007/s00024-024-03436-w

Ribeiro A, Quesada C, Dallmeyer RD (1990) Geodynamic evolution of the iberian massif. In: Dallmeyer RD, Garcia EM (eds) Pre-mesozoic geology of Iberia. IGCP-Project 233. Springer, Berlin, Heidelberg, pp 399–409

Serviços Geológicos de Portugal (1992) Folha Sul da Carta Geológica de Portugal, na escala 1:500 000. 5ª Edição, Serviços Geológicos de Portugal, Lisboa, Portugal, p 1

Süle B, Wéber Z (2013) Earthquake source parameters and scaling relationships in Hungary (central Pannonian basin). J Seismol 17:507–521

Tusa G, Brancato A, Gresta S (2006) Source Parameters of Microearthquakes in Southeastern Sicily, Italy. Bull Seismol Soc Am 96:968–983. https://doi.org/10.1785/0120050071

Tusa G, Gresta S (2008) Frequency-Dependent Attenuation of P Waves and Estimation of Earthquake Source Parameters in Southeastern Sicily. Italy Bull Seism Soc Am 98(6):2772–2794

Wachilala P, Borges J, Caldeira B, Bezzeghoud M (2023) Seismic Sequence Analysis of the Arraiolos Zone, South Portugal, and Its Seismotectonic Implications: A Detailed Analysis of the Period 15 January–30 June 2018. Remote Sens 15:4494. https://doi.org/10.3390/rs15184494

Watanabe K, Sato H, Kinoshita S, Ohtake M (1996) Source characteristics of Small to Moderate Earthquakes in the Kanto Region, Japan: Application of a New Definition of the S-Wave Time Window Length. Bull Seismol Soc Am 86:1284–1291. https://doi.org/10.1785/BSSA0860051284

Zbyszewski G, Carvalhosa AB, Ferreira OV (1979) Carta Geológica de Portugal na Escala 1/50.000. Nota Explicativa da Folha 35–B Mora. 1ª Edição, Serviços Geológicos de Portugal, Lisboa, Portugal, p 33

Zbyszewski G, Carvalhosa AB, Ferreira OV (1980) Carta Geológica de Portugal na Escala 1/50.000. Nota Explicativa da Folha 36–A Pavia. 1ª Edição, Serviços Geológicos de Portugal, Lisboa, Portugal, p 39

Zobin VM, Havskov J (1995) Source spectral properties of small earthquakes in the northern North Sea. Tectonophysics 248:207–218. https://doi.org/10.1016/0040-1951(94)00273-C